Chapter 4

TIO$_2$-PHOTOCATALYZED AS(III) OXIDATION IN A FIXED-BED, FLOW-THROUGH REACTOR

4.1 Abstract

Compliance with the U.S. drinking water standard for arsenic (As) of 10 μg L^{-1} is required as of January 2006. This will necessitate implementation of treatment technologies for As removal by thousands of water suppliers. Although a variety of such technologies is available, most require pre-oxidation of As(III) to As(V) for efficient performance. Previous batch studies with illuminated TiO$_2$ slurries have demonstrated that TiO$_2$-photocatalyzed As(III) oxidation occurs rapidly. This study examined reaction efficiency in a flow-through, fixed-bed reactor that provides a better model for treatment in practice. Glass beads were coated with mixed P25/sol gel TiO$_2$ and employed in an upflow reactor irradiated from above. The reactor residence time, influent As(III) concentration, number of TiO$_2$ coatings on the beads, solution matrix, and light source were varied to characterize this reaction and determine its feasibility for water treatment. Repeated usage of the same beads in multiple experiments or extended use was found to affect effluent As(V) concentrations but not the steady-state effluent As(III) concentration, which suggests that As(III) oxidation at the TiO$_2$ surface undergoes dynamic sorption equilibration. Catalyst poisoning was not observed either from As(V)

or from competitively adsorbing anions, although the higher steady-state effluent As(III) concentrations in synthetic groundwater compared to 5 mM $NaNO_3$ indicated that competitive sorbates in the matrix partially hinder the reaction. A reactive transport model with rate constants proportional to incident light at each bead layer fit the experimental data well despite simplifying assumptions. TiO_2-photocatalyzed oxidation of As(III) was as, if not more, effective with natural sunlight than with a 365 nm lamp. Limitations to the efficiency of As(III) oxidation in the fixed-bed reactor were attributable to constraints of the reactor geometry, which could be overcome by improved design. The fixed-bed TiO_2 reactor offers an environmentally benign method for As(III) oxidation.

4.2 Introduction

Arsenic (As) is implicated in bladder, liver, kidney, and skin cancers (Korte and Fernando 1991; Smith et al. 2002), and the primary exposure route for most people is through ingestion of food and drinking water. For this reason, the U.S. drinking water standard was revised in 2001 from 50 μg L^{-1} to 10 μg L^{-1}. Because elevated As concentrations can occur naturally in groundwater, many water supply facilities will need to implement As removal measures to meet the new standard.

Arsenic in groundwater occurs primarily as arsenite, As(III), or arsenate, As(V). The latter is efficiently removed by several commonly used water treatment methods, including coagulation with ferric chloride or alum, ion exchange, and activated alumina. However, As(III) removal using these processes is often quite poor (McNeill and

Edwards 1995b; Hering et al. 1996; Hering et al. 1997; McNeill and Edwards 1997). Thus, it is typically recommended to oxidize As(III) to As(V) prior to performing standard water treatment procedures. Photocatalyzed As(III) oxidation by titanium dioxide (TiO_2) offers a relatively inexpensive, environmentally benign way to achieve this goal.

TiO_2 is the most extensively used of the semiconductor photocatalysts because of its low cost, biological and chemical inertness, and stability with respect to corrosion. As with other semiconductors, absorption of light with energy greater than or equal to the TiO_2 bandgap energy (3.2 eV or 387 nm) generates charge carrier separation. Recombination of the electron and hole, which generates heat but results in no chemical transformations, may occur either in the bulk solid or at the particle surface (Hoffmann et al. 1995). Alternatively, the electron and hole may migrate to the particle surface, where they can participate in reduction and oxidation reactions with organic and inorganic substrates.

As(III) oxidation using illuminated TiO_2 slurries was first demonstrated by Yang et al. (1999), and this system has since been examined by several groups (Bissen et al. 2001; Lee and Choi 2002; Jayaweera et al. 2003; Ryu and Choi 2004; Dutta et al. 2005; Ferguson et al. 2005; Pena et al. 2005; Xu et al. 2005). The oxidation reaction has been shown to be robust over a wide pH range (Bissen et al. 2001; Lee and Choi 2002; Dutta et al. 2005). At low TiO_2 loadings, the reaction rate constants increase proportionally with loading (Bissen et al. 2001). The overall rate of As(III) oxidation can be pseudo zero-order or pseudo first-order depending on whether the TiO_2 surface is saturated with respect to sorption of As(III) (Ferguson et al. 2005). Addition of Fe(III) and humic acids

was found to enhance As(III) photooxidation (Lee and Choi 2002; Dutta et al. 2005). Experiments using natural sunlight rather than UV lamps were also successful: complete oxidation of 1.33 μM and 26.7 μM dissolved As(III) was observed within 5 and 30 minutes with 0.01 and 0.2 g TiO_2 L^{-1}, respectively (Bissen et al. 2001; Pena et al. 2005).

Despite these promising results, the batch TiO_2 slurry systems studied have limited applicability to water treatment systems. If TiO_2 is to be used in practice for pre-oxidation of As(III) (i.e., prior to subsequent As(V) removal technologies), the TiO_2 must be continuously separated from the water undergoing treatment so that the photocatalyst can be reused. Furthermore, the need to regenerate the photocatalyst must be accommodated. These criteria can be satisfied by either a fluidized-bed or fixed-bed reactor design.

Fixed-bed TiO_2 reactors have been used in many applications in both water and gas-phase treatment systems. Substrates include glass beads (Serpone et al. 1986; Alekabi and Serpone 1988; Wang et al. 1998; Dijkstra et al. 2001; Balasubramanian et al. 2004), stainless steel supports (Fernandez et al. 1995; Balasubramanian et al. 2004), sand (Matthews 1991), quartz (Fernandez et al. 1995; Herrmann et al. 1997), fiber optic cables (Peill and Hoffmann 1996), chitosan beads (Kim et al. 2005), activated carbon (Kim et al. 2005), and immobilization with polymer glue (Grzechulska and Morawski 2003). Glass beads were chosen for this study because of their relatively high surface area and the simplicity of coating procedures. The beads were coated with an amended TiO_2 sol gel that combined strong adhesive properties with high photocatalytic activity (Balasubramanian et al. 2003; Balasubramanian et al. 2004). Using the coated beads in a fixed-bed, flow-through reactor, we examined TiO_2-photocatalyzed As(III) oxidation

with influent As(III) concentrations ranging from 42–620 µg L^{-1} (0.56–8.3 µM) in a simple NaNO$_3$ matrix and in artificial groundwater solutions. This system achieves efficient oxidation of As(III) to As(V) under both UV irradiation and natural sunlight. Inhibition of the photocatalyst activity either by the product As(V) or by the competing sorbents phosphate and fluoride was not observed, suggesting that practical application may be feasible without frequent photocatalyst regeneration.

4.3 Materials and Methods

4.3.1 Bead preparation and characterization

A Degussa P25-doped TiO$_2$ sol-gel was prepared according to a procedure from Balasubramanian et al. (2003). Diethanolamine (Baker Analyzed) was added in a 4:1 molar ratio to 0.5 M titanium (IV) isopropoxide (Ti(OC$_3$H$_7$)$_4$, Sigma-Aldrich) in isopropanol (OmniSolv High Purity Solvent). The resulting mixture was stirred at room temperature for 2 hours. Water (18.2 MΩ, Milli-Q) was then added dropwise to reach a final 2:1 molar ratio of H$_2$O to Ti(OC$_3$H$_7$)$_4$, resulting in a clear anatase sol. Degussa P25 TiO$_2$ was stirred in to achieve a loading of 30.4 g P25 L^{-1}, yielding approximately equal loadings of anatase sol-gel TiO$_2$ and P25 TiO$_2$. This final mixed sol was white in color and was used without further treatment.

Glass beads 5 mm in diameter (Pyrex) were placed in beakers and covered with the sol-gel for 10 minutes before draining and air-drying overnight. They were then placed in a furnace and heated at 100 °C for 1 hour. The furnace temperature was ramped up to 500 °C (~4.5 °C min^{-1}) and maintained at 500 °C for another hour to fix the

sol-gel to the beads. Beads were allowed to cool before repeating the procedure to achieve a total of 1, 4, or 8 coats of TiO_2.

TiO$_2$ crystal structure on the bead surface was identified using X-ray diffraction (XRD, Philips powder diffractometer), and a LEO 1550VP field emission scanning electron microscope was used to determine coating thickness and surface morphology. In preparation for examining coating thickness, beads were immobilized in epoxy, ground down to expose cross sections (Buehler Ecomet 3, 1 μM grinding size), and coated with a 9 nm layer of carbon (Cressington Turbo Carbon Evaporater 208c). To assess surface morphology, beads were immobilized with carbon tape and coated with a 4 nm iridium layer (Cressington Sputter Coater 208 HR).

4.3.2 Preparation of influent solutions

Influent solution was prepared with 0.56–8.3 μM As(III) (Baker Analyzed Reagent, NaAsO$_2$) and 5 mM NaNO$_3$ (Mallinkrodt AR), and adjusted to pH 6.5 using NaOH. Influent flow rate was varied between 1.6–7.6 mL min^{-1}.

Experiments were also conducted using a synthetic groundwater solution spiked with 2.6 μM As(III) at a flow rate of 4.2 mL min^{-1}. Table 4.1 lists the concentrations of major and minor constituents used to prepare a model groundwater solution in Milli-Q water. All salts were analytical grade and were used without further purification. Some experiments were also conducted under high fluoride and phosphate conditions with 1,000 μg L^{-1} (53 μM) fluoride and 75 μg L^{-1} (2.4 μM) phosphate.

Influent solution was continuously stirred and sparged with air before being pumped into the reactor. Samples of influent solution were taken before and after each experiment to ensure that all As entering the reactor was present as As(III).

Table 4.1. Composition of synthetic groundwater matrix.

Species	Concentration[a] mg L^{-1}	μM
HCO$_3$	195	3200
Ca	62.0	1550
Cl	28.9	814
K	6.05	155
Mg	7.78	320
Na	40.9	1780
SO$_4$	30.8	320
SiO$_2$	16.0	266
Cu(I)	0.00197	0.031
F [b]	0.200	10.53
Fe(II)	0.010	0.180
Mn(II)	0.00599	0.109
PO$_4$ (as P) [b]	0.020	0.646
Sr	1.20	13.70
Zn(II)	0.020	0.306
pH	8.4	

a. Concentrations were designed to approximate median groundwater composition as reported by Langmuir (Langmuir 1997) and the USGS (Williamson et al. 2005).

b. Concentrations in high F/PO$_4$ synthetic groundwater: 1 mg L^{-1} F (53 μM) and 75 μg L^{-1} PO$_4$ (as P, 2.4 μM)

4.3.3 Flow-through reactor

The reactor (Fig. A.1, Appendix A) contained two cylindrical chambers separated by a fine nylon mesh. Influent solution entered the lower chamber, where it was stirred to ensure uniform percolation through the mesh screen into the upper chamber. The upper chamber was filled with 6 layers of TiO$_2$-coated beads (149 beads per layer). The pore volume of the bead-filled chamber was 42 mL. The upper chamber was open on top so

the system could be irradiated from above (UVP, 8W, 365 nm). Prior to UV exposure, solution was flowed through the reactor in the dark for 2–6 hours to approach sorption equilibrium and breakthrough of influent concentrations. Effluent dripped through an outlet tube just above the sixth bead layer, and effluent samples were collected intermittently over the course of the run. After the desired run time (usually 3 hours), influent flow was stopped and the reactor was exposed to UV light for 12 more minutes, effectively transforming the reactor into a batch system for that period. After the period of "static" irradiation, a sample was removed by pipetting directly from the reactor. At the end of each photooxidation run, beads were removed and rinsed several times with water before reuse.

An experiment using natural sunlight as the irradiation source was conducted between 12:10 pm and 3:20 pm in Pasadena, CA on September 14, 2005. Procedures followed were identical to UV lamp irradiation experiments, but ferrioxalate actinometry (Calvert and Pitts 1966) was conducted during the same time period to estimate the solar photon flux.

Actinometry was also used to determine the intensity of incident light and the extent of light attenuation with multiple bead layers. Results from 3 to 4 runs using different irradiation periods were averaged for determination of incident light intensity, whereas 2 different irradiation periods were used for bead layer experiments. To determine how much light was transmitted through layers of beads coated 0, 1, 4, or 8 times, beads were placed in a crystallization dish, which was filled with water to a height corresponding to 6 bead layers. A second crystallization dish containing the chemical actinometer was placed beneath the dish containing the beads. The walls of this second

dish were covered to ensure that the actinometer was exposed only to light penetrating through the bead layers.

4.3.4 Arsenic analysis

Samples were analyzed using a liquid column chromatograph (LC, HP Series 1100 isocratic pump) coupled to an inductively coupled plasma mass spectrometer (ICP-MS, HP4500). Samples collected from runs with influent As(III) concentrations of 2.6 μM and 8.3 μM were diluted 3-fold and 10-fold in water. Standards (0.033–1.33 μM, PlasmaCal) were prepared in the same matrix as the samples being analyzed (i.e., 5 mM $NaNO_3$ or synthetic groundwater). The LC injection volume was 50 μL. An anion exchange column (Agilent speciation column with guard column) with an eluent solution of 3.4 mM phosphate, 0.26 mM EDTA, and 2% methanol (pH 6.0) was used to separate As(III) and As(V) peaks, resulting in respective retention times of 2.4 and 7.3 min at a flow rate of 0.9 mL min^{-1}.

4.3.5 Modeling

Geochemist's Workbench 6.0 was used to model the system using one-dimensional reactive transport (X1t). It was assumed that influent solution flows uniformly upward through the first 5 bead layers, then upwards and laterally through the top layer to reach the outlet tube. Therefore, one model was designed to simulate the upward flow, and the output from that model was used as the inlet conditions for a second model representing flow in the top bead layer. Model conditions are listed in Table A.1.

If electron-hole recombination remains constant, the number of reactive charge carriers, and hence the As(III) photooxidation rate, should be proportional to the incident light intensity. Therefore, the light attenuation measurements for different numbers of bead layers were used to scale the rate constant (Table A.2).

Since photocatalytic oxidation of As(III) occurs at the TiO_2 surface, the reaction rate should be expressed as a function of the adsorbed As(III) concentration. However, this parameter is not experimentally accessible. In modeling batch experiments (Ferguson et al. 2005), dissolved As(III) concentration was used as a proxy for adsorbed concentration, which is appropriate if the sorption reaction is at pseudo equilibrium. That approach was also followed in this study.

With these simplifications, the TiO_2-photocatalyzed As(III) oxidation was simulated using the solution-phase reaction:

$$As(OH)_3 + 0.5\ O_2 \rightarrow H_2AsO_4^- + H^+ \tag{4.1}$$

Since the influent solution was air-saturated, the system was modeled as pseudo first-order in the dissolved As(III) concentration. Note that, because sorption to TiO_2 is not explicitly included in the simulation, inhibition by competitive product sorption cannot be modeled.

4.4   Results and Discussion

4.4.1   Bead characterization

XRD spectra (Fig. A.3) indicated that the TiO_2 coating on the beads was 81–85% anatase and 15–19% rutile. This ratio is slightly less than that of P25 powder, which is 20-30% rutile. Such a dilution of the rutile:anatase ratio would be expected from the mixture of sol-gel TiO_2 and P25. No differences in TiO_2 composition were observed between the 4x and 8x coated beads, indicating that the 500 °C heating step between coatings did not significantly alter the rutile:anatase ratio.   XRD spectra also included a small quartz signal due to the glass bead support.

The total TiO_2 thickness on beads with 1, 4, or 8 coatings ranged from 2 to 30 μm. Beads with more coatings had a greater average thickness, but substantial heterogeneity in the surface thickness was observed, probably due to clusters of P25 spread unevenly throughout the sol (Fig. A.4). Figure 4.1 depicts the surface morphology of the TiO_2-coated beads. In Figure 4.1a, several layers and surface cracking are evident. At greater magnification (Fig. 4.1b), it is clear that the TiO_2 particles are present as discrete nanoparticles of about 15 nm diameter. No microcracks are visible at this magnification.

4.4.2   System performance

Each photooxidation experiment was preceded by a period during which the TiO_2-coated beads were equilibrated with the influent solution in the dark. During the dark equilibration period, effluent As(III) concentrations ($[As(III)]_{out}$) decreased due to sorption onto the TiO_2 and then gradually increased (Fig. A.5). Equilibration between dissolved and adsorbed As(III), indicated in this system by breakthrough of influent
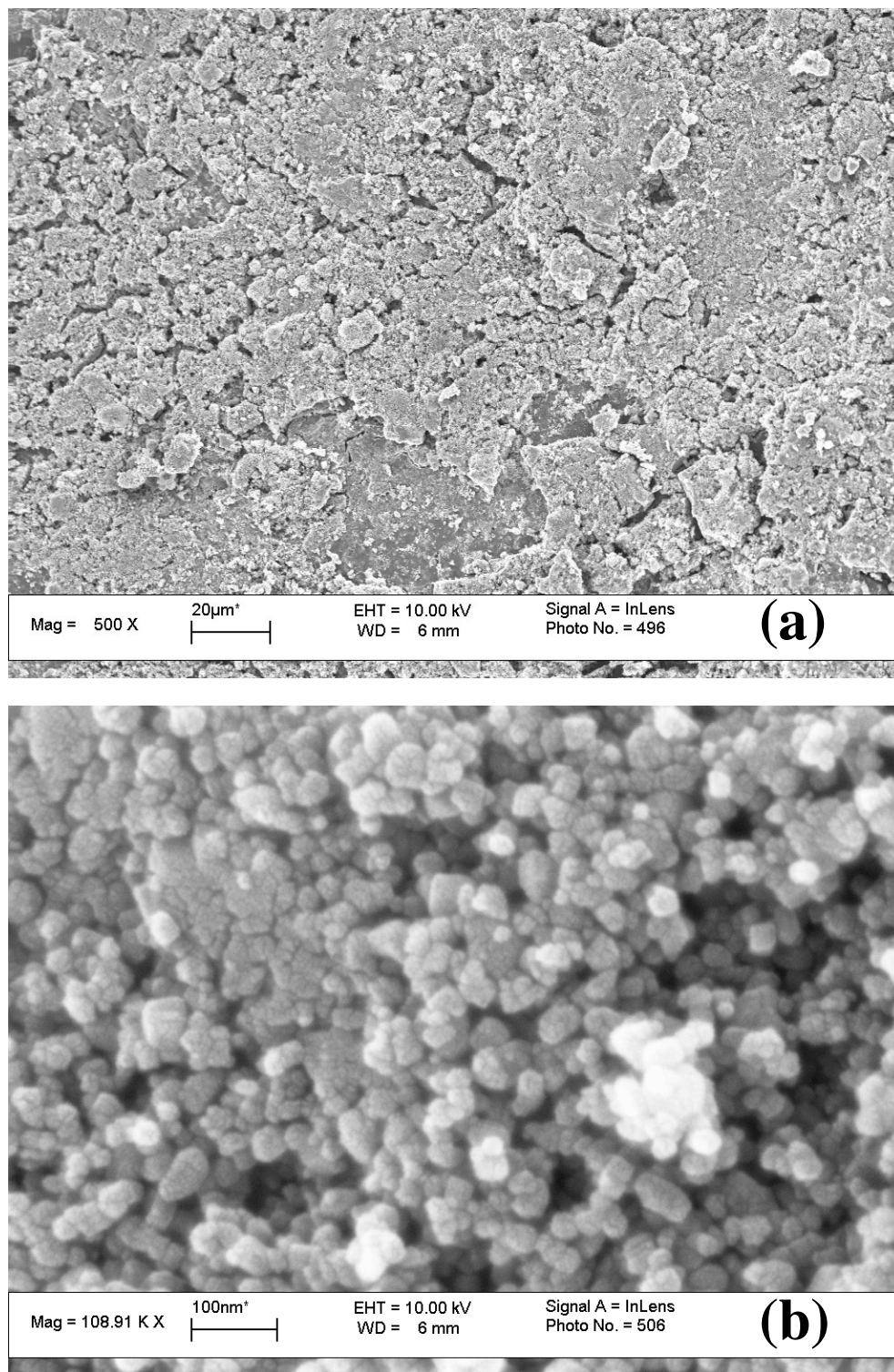
Figure 4.1. SEM micrographs of beads coated 8 times with P25-doped sol-gel at (a) 500x magnification and (b) 109kx magnification. Conditions: electron high tension = 10 kV, working distance = 6 mm, In-Lens detector.

[As(III)], required longer than in batch studies (Ferguson et al. 2005) due to the continual displacement of fluid.

When UV exposure was initiated, $[As(III)]_{out}$ decreased rapidly, reaching a constant value after 10-30 minutes. As(V) was also observed in the reactor effluent at concentrations ($[As(V)]_{out}$) that increased over the course of the experiment (Fig. 4.2). The breakthrough of As(V) was strongly affected by the number of times the beads were used. For new beads, there was no As(V) in the effluent at the end of the dark equilibrium period (i.e., at $t = 0$). However, this was not the case for re-used beads because the water rinses between experiments did not completely desorb As(V) from the TiO_2. The value of $[As(V)]_{out}$ at $t = 0$ increased with greater extent of previous bead use. $[As(V)]_{out}$ also increases more rapidly toward its steady-state value with increasing number of prior uses. This suggests that As(V) breakthrough is strongly influenced by sorption-desorption at the TiO_2 surface. Consistent with this behavior, the prior use of the beads also affected the changes observed in $[As(V)]_{out}$ when flow was stopped. As illumination continued under static conditions, the combination of photochemical production and sorption-desorption of As(V) led to a net increase in $[As(V)]_{out}$ for beads used 3 or 5 times and a net decrease in $[As(V)]_{out}$ for beads used only once or for new beads.

The dark sorption period needed to achieve breakthrough of influent As(III) concentrations demonstrated a similar dependence on previous bead usage. New beads required 6 hours to achieve $[As(III)]_{out}$ within 10-20% of influent concentrations ($[As(III)]_{in}$), whereas beads that had been used 4 or more times previously showed influent breakthrough within 1–2 hours. However, prior usage of the beads had little

effect on the steady-state value of [As(III)]$_{out}$. Comparable steady-state values of [As(III)]$_{out}$ were observed with new beads and with beads used 1 or 3 times (Fig. 4.2). Although a slightly higher steady-state value of [As(III)]$_{out}$ was observed for beads used 5 times, when this data set was compared with other sets of experiments, no consistent trend was discernible in steady-state [As(III)]$_{out}$ as a function of previous bead usage (Table A.3).
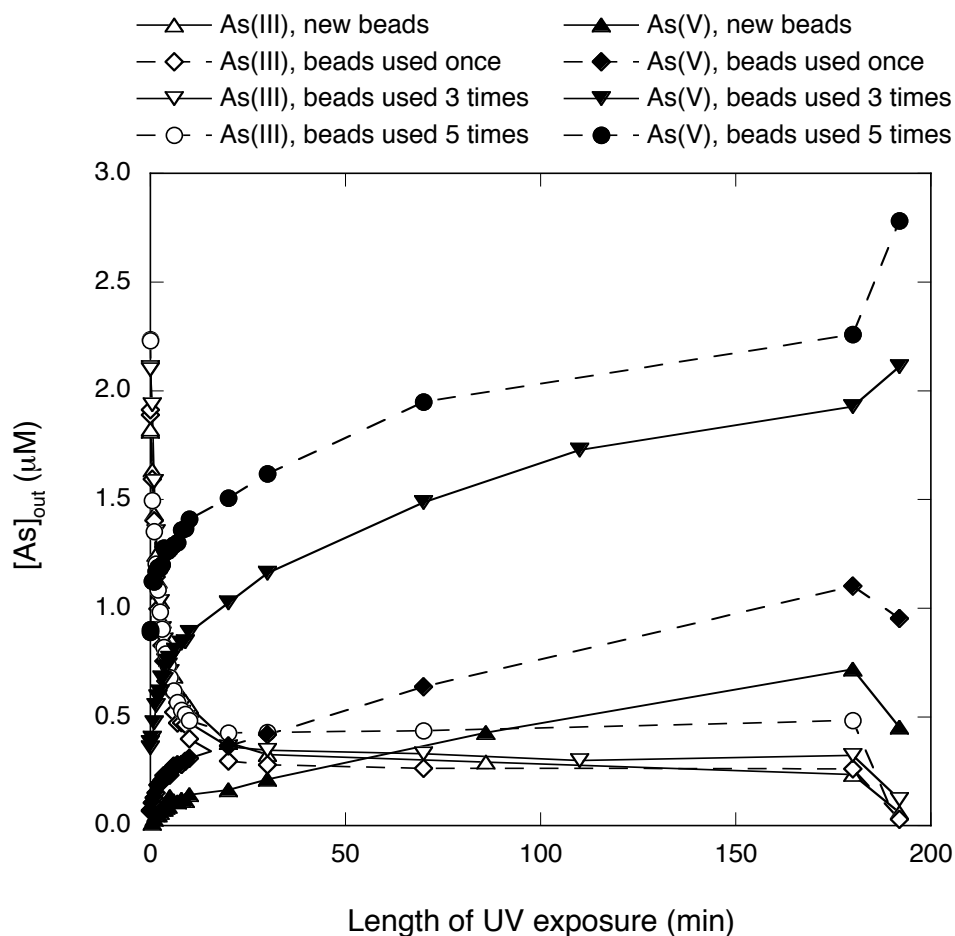

Figure 4.2. Effect of previous bead use on loss of As(III) (open symbols) and increase of As(V) (closed symbols) during UV exposure. Conditions: pH 6.4, [As(III)]$_{in}$ = 2.6 μM, [NaNO$_3$] = 5 mM, average residence time = 10 min, 4x coated beads.

The patterns observed in the As(III) breakthrough curves during dark equilibration and $[As(V)]_{out}$ during illumination indicated that As(V) does accumulate to some extent on the TiO_2 surface with extended or repeated use of the beads. This did not, however, appear to diminish the effectiveness of As(III) oxidation, as shown by the constant values of the steady-state $[As(III)]_{out}$ observed with repeated or extended use. The rate of desorption of As(V) appears to be sufficient to prevent irreversible poisoning of the photocatalyst.

4.4.3 Dependence on O_2

The experimental design (specifically the sparging of the influent solution with air prior to its introduction into the reactor) was intended to avoid any O_2 limitation of the As(III) photooxidation reaction. Dissolved O_2 is required as an electron acceptor for the photocatalytic reaction (Yang et al. 1999). Under conditions of O_2 limitation, trapped electrons remain on the TiO_2 surface and enhance the rate of electron-hole recombination, which decreases photocatalyst activity. Although the saturation of the influent solution with air (nominal dissolved $[O_2] = 0.26$ mM) should be sufficient to avoid O_2 limitation, this was confirmed under static conditions, where the flow through the reactor was halted at the end of each experiment and UV irradiation was continued for another 12 minutes. If the reaction was limited by O_2, the concentration of dissolved As(III) in the reactor would be expected to remain constant. Instead, As(III) concentrations decreased to trace levels, demonstrating that sufficient O_2 was available to drive the photooxidation reaction to completion (Fig. 4.2).

4.4.4 Effect of multiple TiO$_2$ coatings

Experiments were conducted with beads coated with 1, 4, or 8 layers of the mixed P25/sol-gel. As the number of coatings increased, the time required for As(III) breakthrough during dark equilibration increased and the values of [As(V)]$_{out}$ decreased. This is consistent with an increase in sorption capacity with increased number of coatings. However, number of TiO$_2$ coatings had no effect on the steady-state value of [As(III)]$_{out}$ (Fig. A.6), indicating that the photocatalytic oxidation of As(III) to As(V) was not enhanced by increasing the number of coatings on the beads. Small differences were observed during the initial period of illumination before the steady-state value of [As(III)]$_{out}$ was attained; the time required to achieve steady-state [As(III)]$_{out}$ increased with the number of TiO$_2$ coatings. This may reflect mass transfer limitations between surface and bulk species, but this cannot be confirmed with the available data.

Since extent of TiO$_2$ coating is expected to affect the amount of light the beads absorb, actinometry was performed to determine the photon flux penetrating successive bead layers (Fig. 4.3). Some light absorption and scattering was observed even with uncoated beads, but substantially greater attenuation was observed with the TiO$_2$-coated beads. A majority of the incident radiation was attenuated with a single layer of beads (70% with beads coated once, 87% with beads coated 4 or 8 times). Less than 4% of the incident light was transmitted through 4 or more layers of even singly coated beads, suggesting that the majority of As(III) oxidation occurs in the top few layers. Light attenuation with beads coated 4 and 8 times was greater than that with beads coated only once despite similar photoactivities of all coated beads. The larger number of photons absorbed, and hence potential photoreactivity, of beads coated 4 and 8 times may be

offset by reduced reaction efficiency from enhanced charge carrier recombination (Egerton and Tooley 2004).
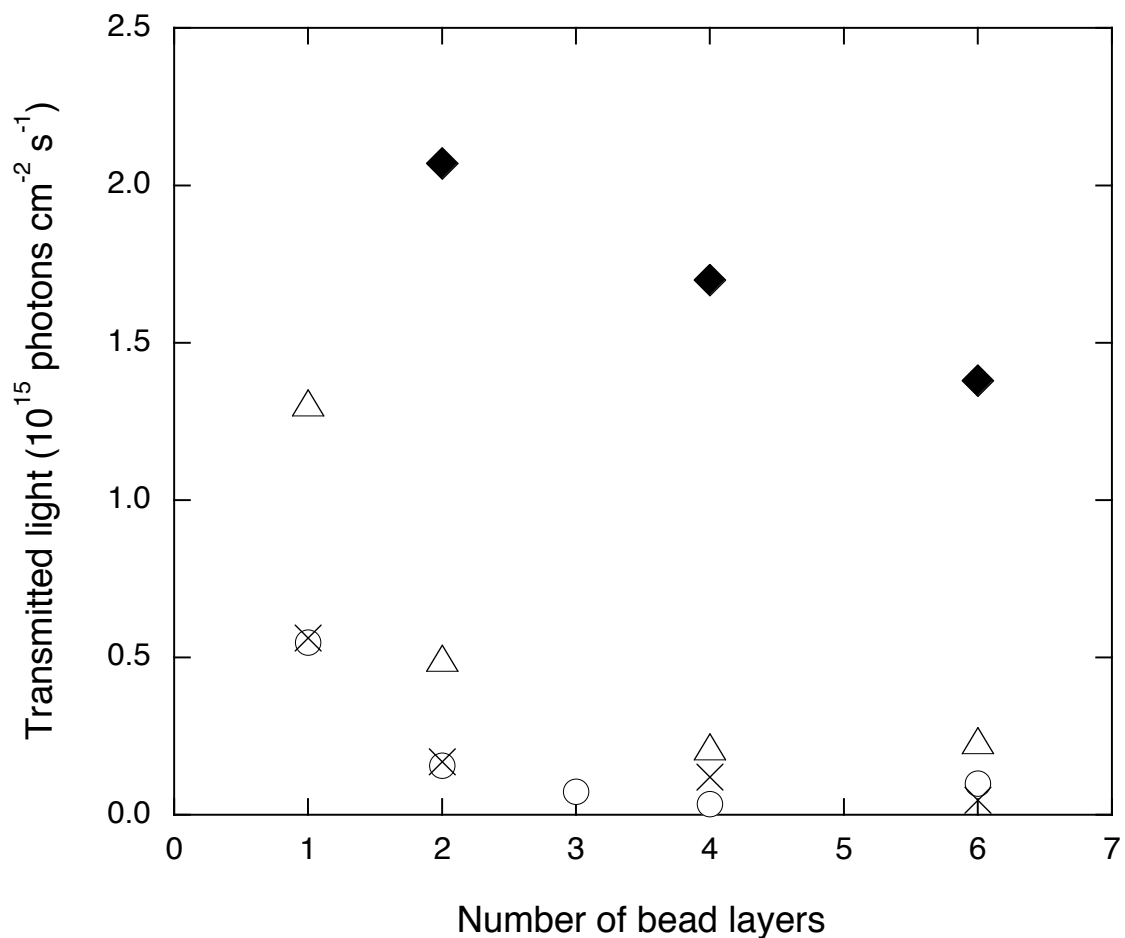

Figure 4.3. Transmitted photon flux through successive layers of uncoated glass beads (◆) and beads with 1 (△), 4 (○), and 8 (✕) TiO$_2$ coatings. Incident photon flux = 4.3 × 10^{15} photons cm^{-2} s^{-1}.

4.4.5   Effect of residence time

The influent flow rate was varied to examine the effect of residence time on As(III) oxidation performance. As seen in Figure 4.4, the value of steady-state [As(III)]$_{out}$ decreased with increasing residence time up to a residence time of 15.6

minutes but did not decrease further for a residence time of 26.3 minutes. A comparison with experiments conducted in the same reactor but under static conditions indicates that the As(III) photooxidation reaction should reach completion in less than 20 min.

This discrepancy can be attributed to the geometry of the reactor and specifically to the fact that the effluent solution exits the reactor from one side. Consequently, there is a distribution of residence times, where fluid entering the upper chamber on the same or opposite side as the effluent port experiences residence times that are shorter or longer, respectively, than the average. Flow studies with KBr as a conservative tracer have confirmed this pseudo normal distribution with tails at 2 and 10 minutes for an average residence time of 5.85 minutes (Fig. A.7). These considerations of flow geometry were incorporated into the model for As(III) oxidation, in which the reaction rate was taken to be pseudo first-order in the dissolved As(III) concentration. The rate constant for As(III) oxidation in the model was adjusted to fit the experimental observations of $[As(III)]_{out}$ for the shortest reactor residence time, which exhibits the greatest sensitivity to this parameter. The fit to experimental data is good for residence times of 10 and 15.6 minutes, but observed steady-state $[As(III)]_{out}$ for a residence time of 26.3 min is higher than predicted (Fig. 4.4). This discrepancy may indicate a transition into a mass transfer-limited regime. In addition, faster than average fluid velocities at the reactor walls may decrease the extent of As(III) oxidation. As particle size increases, fluid is more likely to flow preferentially along the wall of the reactor due to increased porosity as the particle packing structure is disrupted. Based on the bead size used in this study, up to 2% of the total flow could travel preferentially along the reactor wall near the outlet, resulting in "short-circuiting" of the reactor (White and Tien 1987; Hunt and Tien 1988).
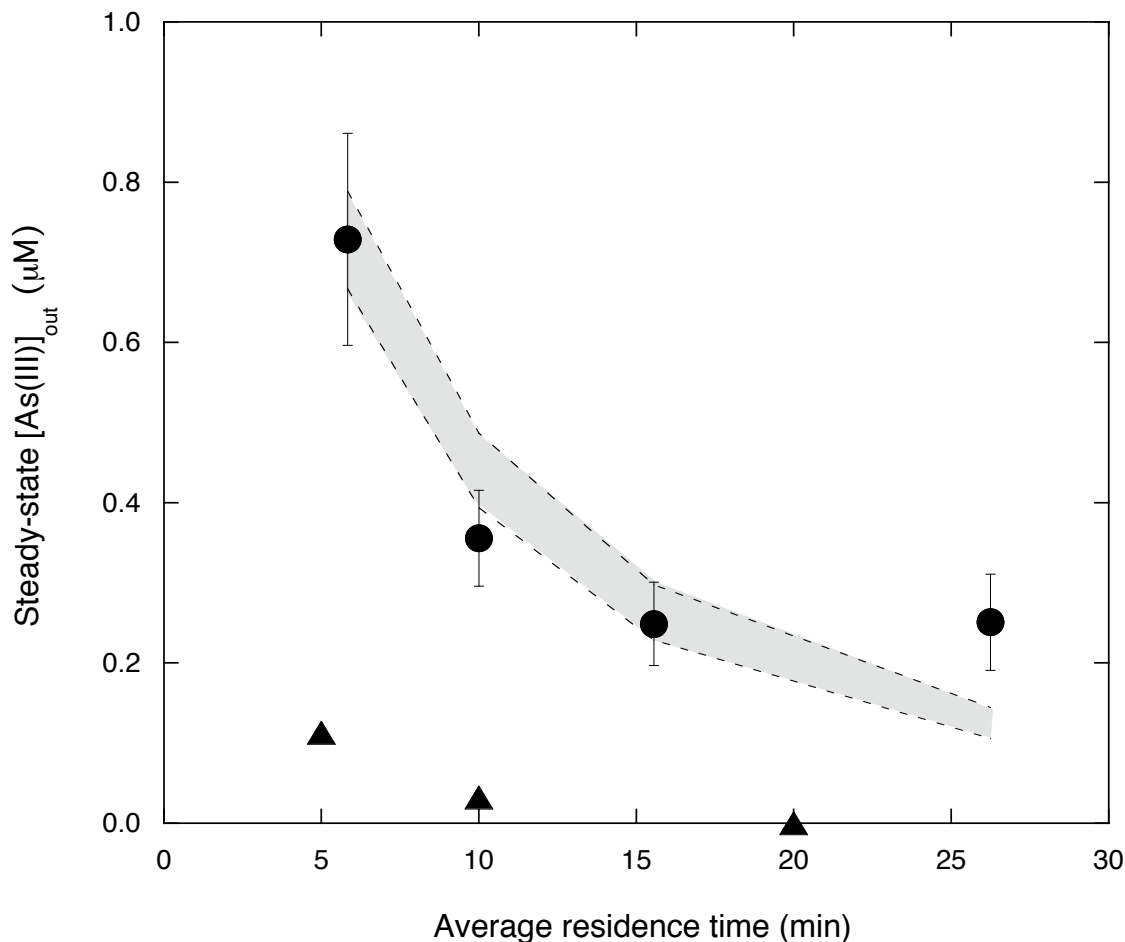
Figure 4.4. Steady-state $[As(III)]_{out}$ (●) as a function of average reactor residence time with error bars representing one standard deviation based on 3–5 replicate experiments. Model results fitted to the shortest residence time are shown with an envelope of ± 10 % variation in the rate constant indicated by dashed lines. Also shown are $[As(III)]_{dissolved}$ values for a static system (▲), in which the influent flow was turned off just before UV irradiation. Conditions: pH 6.4, $[As(III)]_{in}$ = 2.64 µM, $[NaNO_3]$ = 5 mM, 4x coated beads.

The successful fit of the model to the data indicates that the simplifications made are sufficient to predict steady-state $[As(III)]_{out}$ for residence times shorter than 16 min. The fitted first-order rate constant for the overall reactor is 0.0111 s^{-1}. This corresponds to a rate constant of 0.0097 s^{-1} for the top bead layer, which is exposed to the full incident light intensity and is therefore the best approximation for the true photooxidation rate constant. This value is about two times greater than the pseudo first-order rate constant

observed in TiO$_2$ slurry studies under similar conditions (0.0048 s^{-1} for 0.05 g L^{-1} P25 TiO$_2$) (Ferguson et al. 2005); however, the rate constant from the slurry studies was considered a lower bound because all incident light was absorbed within the first few centimeters of the reactor, causing the back of the reactor to function as dead volume.

Because the model does not explicitly include sorption, it cannot predict the concentrations of As(V) in the reactor effluent. The dependence of [As(V)]$_{out}$ on the prior use of the beads and the changes in [As(V)]$_{out}$ during the static period at the end of the flow-through experiment clearly indicate that sorption must be included to predict [As(V)]$_{out}$ accurately. However, it is the breakthrough of (unreacted) As(III) that is of primary concern since the presence of As(III) in the reactor effluent will compromise the performance of downstream unit operations that remove As(V) more effectively than As(III).

4.4.6   Effect of [As(III)]$_{in}$

For a given residence time, the concentration of the reactant undergoing a first-order reaction should be directly proportional to its initial concentration. Figure 4.5 shows that as [As(III)]$_{in}$ increases, steady-state [As(III)]$_{out}$ deviates from this expected linear relationship. This is consistent with previous batch studies performed with TiO$_2$ slurries, in which a transition from first-order to zero-order dependence on the dissolved [As(III)] was observed as the initial [As(III)] increased from 2.5 to 42 μM. This was attributed to saturation of sorption sites on the TiO$_2$ surface, which caused a transition from the linear region to the plateau region of the sorption isotherm (Ferguson et al. 2005). The same mechanism appears to apply here, but because the coated beads used in

this study have a significantly smaller surface area than TiO_2 slurries, the As(III) concentration at which surface saturation and transition to zero-order kinetics occurs is lower for this study (i.e., 8.3 μM rather than 42 μM).

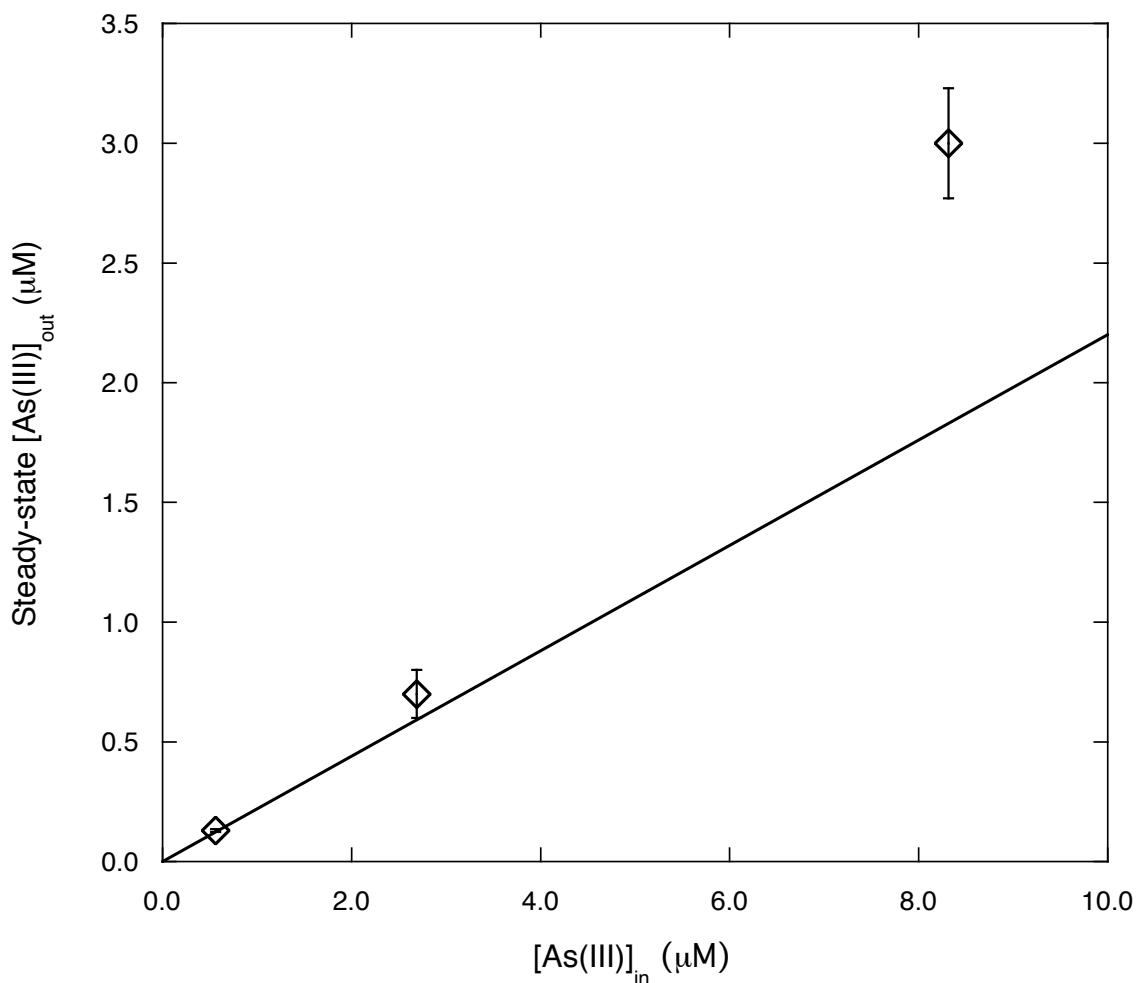**Figure 4.5.** Steady-state [As(III)]$_{out}$ as a function of [As(III)]$_{in}$ compared to the linear response expected for a reaction that is pseudo first-order in As(III). Conditions: pH 6.4, [NaNO$_3$] = 5 mM, average residence time = 5.85 min, 4x coated beads. Error bars represent one standard deviation based on 3–4 replicate experiments.

The lowest value of [As(III)]$_{in}$ shown in Figure 4.5 ([As(III)]$_{in}$ = 0.56 μM = 42 μg L^{-1}) is within the relevant range for water systems whose raw water supplies met the

previous U.S. drinking water standard for As but exceed the current standard. At this concentration, an average residence time of only 5.85 minutes generated a product water with $[As(III)]_{out}$ of 0.13 μM (9.7 μg L^{-1}). Thus subsequent removal of As(V) (present at 0.45–0.56 μM or 34–42 μg L^{-1}) from the photocatalytically pre-treated water would result in a final As concentration that would meet the drinking water standard. The extent of As(III) oxidation could be increased by lengthening the reaction time (e.g., up to 15 min, Fig. 4.4) or by changing the reactor geometry to use the incident radiation more effectively as described below.

4.4.7 Effect of a groundwater matrix on As(III) oxidation

Although As(III) in a simple $NaNO_3$ matrix was observed to be readily photooxidized by TiO_2 in a fixed-bed reactor, the presence of competing sorbates like phosphate and fluoride might be expected to interfere with As(III) photooxidation and possibly even result in irreversible poisoning of the photocatalyst. To examine these effects, experiments were conducted with synthetic solutions representative of median U.S. groundwater and a high fluoride, high phosphate groundwater (Table 4.1). The 2-unit pH difference between synthetic groundwater solutions and $NaNO_3$ solutions was not expected to significantly affect the reaction based on observations from previous studies conducted over a wide pH range (Bissen et al. 2001; Lee and Choi 2002; Dutta et al. 2005). As shown in Figure 4.6, the steady-state values of $[As(III)]_{out}$ are higher in the synthetic median groundwater than in the $NaNO_3$ matrix, indicating impaired performance of the photocatalyst under these conditions. However, further increases in the phosphate concentration (by a factor of 3.75) and fluoride concentration (by a factor
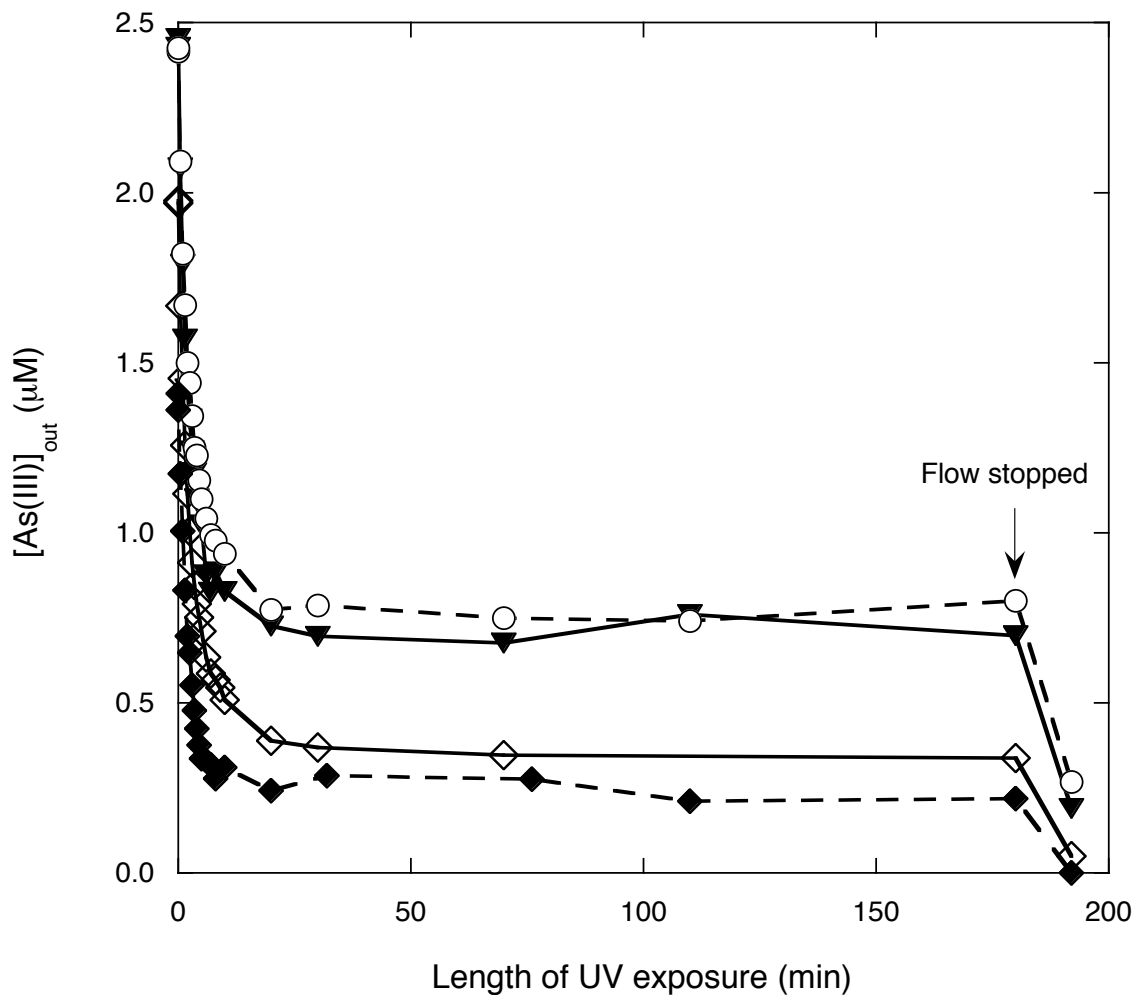
Figure 4.6. As(III) oxidation comparison among different water matrices and light sources: 5 mM $NaNO_3$ / UV lamp ($\diamond$), synthetic groundwater / UV lamp ($\blacktriangledown$), synthetic groundwater with 53 μM fluoride and 2.4 μM phosphate / UV lamp ($\bigcirc$), and synthetic groundwater / natural sunlight ($\blacklozenge$). Conditions: pH 8.4 (groundwater) or 6.4 ($NaNO_3$), $[As(III)]_{in}$ = 2.6 μM, average residence time = 10 min, 4x coated beads. Error bars represent one standard deviation based on 3–5 replicate experiments.

of 5) had no significant effect on performance. Thus, the much higher bicarbonate concentration (3.2 mM) may be the primary reason for reduced catalyst performance. Bicarbonate most likely inhibits As(III) photooxidation by competitive sorption, but it is also a weak hydroxyl radical scavenger ($k = 1 \times 10^7$ M^{-1} s^{-1} (Buxton et al. 1988b).

During the static UV illumination period at the end of the flow-through experiment, the dissolved As(III) concentration in the reactor run with synthetic groundwater solutions decreased, but not to the level observed with the $NaNO_3$ matrix. Again, little difference was observed between the median and high fluoride/phosphate groundwater solutions. In addition, a groundwater matrix experiment that was extended for 24 hours showed no change in steady-state $[As(III)]_{out}$ over time, indicating that poisoning on this time scale is not an issue even for a system with more competitively adsorbing ions available. Development of a light brown-orange tinge was observed on the beads over time due to Fe(III) precipitation, but this had no effect on steady-state $[As(III)]_{out}$.

The average value of $[As(V)]_{out}$ was higher for experiments using synthetic groundwater compared to those using a 5 mM $NaNO_3$ matrix (Table A.3), suggesting that the presence of competing ions inhibits As(V) sorption to the TiO_2. However, the magnitude of this effect is not clear because previous bead usage has a strong effect on $[As(V)]_{out}$. Comparison between matrices is confounded by the large experimental variability associated with varying prior use of the beads.

4.4.8   Reaction under natural sunlight

Also plotted in Figure 4.6 are the results from an experiment conducted in the median groundwater matrix under natural sunlight. The steady-state value of $[As(III)]_{out}$ under these conditions was lower than those observed under 365 nm UV irradiation of either the groundwater or $NaNO_3$ matrix. Ferrioxalate actinometry showed that total photon flux in the ferrioxalate-active region (300–580 nm) was about 5 times higher than

corresponding lamp photon flux; however, when adjusted to account only for wavelengths lower than the bandgap cutoff for TiO_2, the ratio of solar photon flux to lamp flux was 2.1:1. This observation emphasizes that the required UV flux needed for this photoreaction is small.

4.4.9 Implications for water treatment

Photocatalyzed oxidation of As(III) to As(V) was demonstrated in a fixed-bed TiO_2 reactor for both a simple $NaNO_3$ matrix and synthetic groundwater solutions. Poisoning of the photocatalyst either by the reaction product As(V) or by competing sorbates in the synthetic groundwater, particularly PO_4 and F, was not observed. This is a critical point because a fixed-bed catalyst must operate over an extended period to be practical for full-scale operation.

Compared with other As(III) oxidation methods, TiO_2 photocatalysis is advantageous in that no hazardous or corrosive chemicals are required. However, costs are also an important consideration. Lamp purchase and energy requirements represent a major cost associated with TiO_2 photocatalysis, but UV lamps have been previously recommended by the U.S. Environmental Protection Agency for use in small water supply systems, in part due to their relatively low cost (US EPA 2003b). Since the current application requires lower UV doses than disinfection, cost estimates for disinfection constitute an upper bound for lamp and electricity costs for TiO_2 photocatalysis. Additional costs for TiO_2 photocatalysis would be associated with installation of the TiO_2 fixed-bed reactors. For groundwaters containing insufficient dissolved O_2 to support

TiO_2-photocatalyzed oxidation of As(III), aeration would be required prior to UV irradiation.

As(III) photooxidation was as, if not more, efficient under natural sunlight than under UV irradiation. Although use of natural sunlight is unlikely to be attractive in developed countries, it may be a viable approach in developing countries where energy costs are a greater consideration.

This study provides a basis for improving and scaling up the TiO_2 fixed-bed reactor. The artifacts of reactor geometry observed in this study could be avoided by using an annular reactor. Since almost all the incident light is absorbed in the first 3 layers of TiO_2-coated beads, additional bead layers can be eliminated. Also, multiple bead coatings are unnecessary since they do not confer any significant improvement in activity. However, since SEM micrographs of beads coated only once indicated that the TiO_2 did not adhere uniformly, 1 or 2 additional coatings may be advisable to ensure complete coating.

This study has yielded promising results that indicate that fixed-bed TiO_2 photocatalysis could be a viable option for the pre-oxidization of As(III) to As(V) prior to treatment for As(V) removal. The relatively low materials cost, minimal chemical requirements, and simple operation make this treatment alternative particularly attractive to small water supply facilities with limited capital and workforce. Although TiO_2-photocatalyzed As(III) oxidation does not directly remove As from water, the As(V) produced can be removed by a variety of conventional treatment technologies.

4.5 Acknowledgements

SUPPORTING INFORMATION AVAILABLE (APPENDIX A)

Includes reactor schematic, model parameters, additional SEM and XRD data, residence time characterization of the reactor, and additional data for flow-through As(III) oxidation experiments.